CHALMERS
FINITE ELEMENT CENTER

PREPRINT 2002–03

Stability of explicit-implicit hybrid time-stepping schemes for Maxwell's equations

Thomas Rylander and Anders Bondeson

Chalmers Finite Element Center
CHALMERS UNIVERSITY OF TECHNOLOGY
Göteborg Sweden 2002

CHALMERS FINITE ELEMENT CENTER

Preprint 2002–03

Stability of explicit-implicit hybrid time-stepping schemes for Maxwell's equations

Thomas Rylander and Anders Bondeson

CHALMERS

Chalmers Finite Element Center
Chalmers University of Technology
SE–412 96 Göteborg Sweden
Göteborg, March 2002

Stability of explicit-implicit hybrid time-stepping schemes for Maxwell's equations
Thomas Rylander and Anders Bondeson
NO 2002–03
ISSN 1404–4382

Chalmers Finite Element Center
Chalmers University of Technology
SE–412 96 Göteborg
Sweden
Telephone: +46 (0)31 772 1000
Fax: +46 (0)31 772 3595
www.phi.chalmers.se

Printed in Sweden
Chalmers University of Technology
Göteborg, Sweden 2002

STABILITY OF EXPLICIT-IMPLICIT HYBRID TIME-STEPPING SCHEMES FOR MAXWELL'S EQUATIONS

THOMAS RYLANDER AND ANDERS BONDESON

Abstract. An improved version of the stable FEM-FDTD hybrid method [T. Rylander and A. Bondeson, "Stable FEM-FDTD hybrid method for Maxwell's equations," *Comput. Phys. Comm.* **125**, 75 (2000)] for Maxwell's equations is presented. The new formulation has a modified time-stepping scheme and is rigorously proven to be stable for time steps up to the stability limit for the FDTD. The new scheme gives less reflection at the boundary between the structured and unstructured grids than the original formulation. The hybrid method is compared to the FDTD with stair-casing for scattering from a conducting sphere. The discretization errors of the hybrid show quadratic dependence on mesh size, while the scaling is less clear for the FDTD. The FDTD gives errors that are 5 - 60 times higher than the hybrid, depending on resolution and stair-casing strategy.

1. Introduction

Each of the two main methods in time-domain Computational Electromagnetics, the Finite-Difference Time-Domain (FDTD) [1, 2] and Finite Element Method (FEM) [3] with edge elements [4], has advantages and disadvantages. The FDTD is very efficient, because it is explicit and simple. However, it has difficulties with oblique and curved boundaries, where stair-casing is the standard solution. Finite elements with tetrahedral grids, on the other hand, are well suited for modeling complex geometry. However, the time-stepping is generally implicit and the method has much higher operation count and memory requirement than the FDTD.

Hybrids have been formulated [5, 6, 7, 8], with the goal of combining the advantages of the two basic methods. To maximize efficiency, such hybrids use FDTD in as large a volume as possible, and finite elements in thin layers near boundaries that do not fit on the FDTD grid. Early versions of FEM-FDTD hybrids [5, 6, 7] suffered from instabilities known as late time growth. These instabilities were typically stabilized by means of dissipative schemes for time-stepping.

Our hybrid method [8] eliminates the instabilities without recourse to dissipation. The key to stability was to derive the spatial operators for the edges at the interface between the

Date: March 20, 2002.

Key words and phrases. FEM, FDTD, stair-case approximation, explicit-implicit time-stepping, hybrid scheme, stability, scattering, Maxwell's equations.

Thomas Rylander, Department of Electromagnetics, Chalmers University of Technology, S–412 96 Göteborg, Sweden, *email*: rylander@elmagn.chalmers.se

Anders Bondeson, Department of Electromagnetics, Chalmers University of Technology, S–412 96 Göteborg, Sweden, *email*: elfab@elmagn.chalmers.se.

FEM and FDTD regions by FEM techniques. It was noted in [8] that the FDTD scheme can be constructed by FEM techniques; Galerkin's method was applied to edge elements on bricks, and the matrices were "lumped", or equivalently, calculated by trapezoidal integration. This procedure gives symmetric matrices for the spatial operators even at the FEM-FDTD interface. Symmetric, real matrices have real eigenvalues, and this removes the source of instabilities occurring when the two types of grid are joined by more ad hoc approaches.

A second order accurate scheme for general geometry has been introduced by Dridi et al. [9] using interpolation points at boundaries. However, Ref. [9] does not prove stability and reciprocity of this scheme, and the simulations shown in [9] are over relatively short time intervals. Ref [10] describes a method using overlapping grids and ficitious points to match solutions in different regions meshed by different structured grids. The approach aims at high accuracy, but appears very demanding to apply in complex geometries.

There are other methods related to the FDTD scheme which are stable and combine efficiency with body-conforming capabilities. Weiland and coworkers have investigated stable local refinement and non-orthogonal grids for the FDTD scheme [11, 12]. Gwarek and coworkers have developed the Transmission Line Method (TLM) to treat complex boundaries by cutting cells [13]. However, our FEM-FDTD hybrid method is generally more flexible and it allows for local spatial refinement without reducing the global time-step. Such local refinement is useful to resolve small geometric details and rapid variations in the fields.

In the present paper, we present an improved time-stepping algorithm for the hybrid method. The new algorithm incorporates FEM ideas also in the time-stepping. The new scheme allows a simple proof of stability. A practical advantage of the new algorithm is that it reduces the reflection at the interface between structured and unstructured grids. Both the new scheme and the stability proof are of rather general nature, and could be applied to similar hybrids for other equations, e.g., in acoustics or solid mechanics. We present several different tests of the new method, comparing it both with the stair-cased FDTD and with the original version of the hybrid. For scattering by a conducting sphere, the hybrid is clearly superior to the FDTD.

2. The hybrid method

2.1. **Spatial discretization.** Our hybrid method uses unstructured layers of tetrahedrons close to complex boundaries, while large volumes are discretized by structured brick elements (typically cubes). The connection between the two types of elements is made by a single layer of pyramids. The pyramids make it possible to expand the solution in edge elements, whose tangential components are continuous everywhere.

Maxwell's equations $\nabla \times \mu^{-1} \nabla \times \vec{E} + \epsilon \partial_t^2 \vec{E} = -\partial_t \vec{J}$ are solved by expanding the electric field in edge elements $\vec{E}(\vec{r}, t) = \sum_i e_i(t) \vec{N}_i(\vec{r})$ and applying Galerkin's method. This gives $\mathbf{S}\mathbf{e}(t) + \mathbf{M}\, \partial_t^2 \mathbf{e}(t) = \mathbf{f}(t)$, where the stiffness (or curl-curl) matrix $S_{ij} = \int \mu^{-1} \nabla \times \vec{N}_i \cdot \nabla \times \vec{N}_j dv$ is symmetric and positive semi-definite, and the mass (or epsilon) matrix $M_{ij} = \int \epsilon \vec{N}_i \cdot \vec{N}_j dv$ is symmetric and positive definite. The FDTD algorithm is also found by this

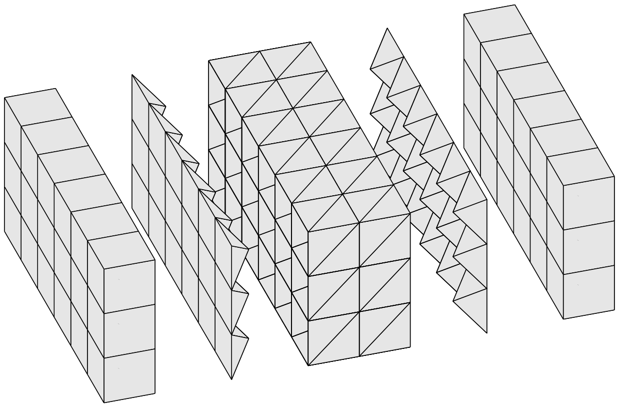

FIGURE 1. Simple hybrid grid.

approach, if the mass and stiffness matrices are lumped. This corresponds to applying the trapezoidal rule for the integration over the bricks. The properties of the matrices $\mathbf{S}$ and $\mathbf{M}$ implies that the eigenvalues ω^2, of $\mathbf{Se} = \omega^2\mathbf{Me}$, are all real and non-negative. Therefore, it is possible to construct a stable time stepping algorithm.

2.2. **Time-stepping.** We emphasize that, in our hybrid scheme, the switch between FDTD and FEM (which is done by the integration method) is linked to the *finite elements* and not the *edges*, or unknowns. Thus, the edges at the interface will neither be treated as regular FEM or regular FDTD. In the first version of the hybrid [8], the switch of time-stepping scheme was, however, made on the basis of the edges; edges interior to the structured grid were time-stepped explicitly and those belonging to the pyramids or tetrahedrons were time-stepped with the implicit algorithm [14]:

$$\mathbf{S}\left[\theta\mathbf{e}^{(n+1)} - (2\theta-1)\mathbf{e}^{(n)} + \theta\mathbf{e}^{(n-1)}\right] + \frac{1}{\Delta t^2}\mathbf{M}\left[\mathbf{e}^{(n+1)} - 2\mathbf{e}^{(n)} + \mathbf{e}^{(n-1)}\right] = 0. \tag{2.1}$$

The algorithm (2.1) is stable for arbitrarily large time-steps if $\theta \geq 1/4$. An important advantage of the implicit FEM part is that the time step need not be reduced if some tetrahedrons are made very small. This allows for adaptivity and good resolution of small geometrical details with only a modest increase of the computational work.

In the original version of the hybrid, we applied the same implicitness parameter θ to all the implicit *edges*. Concerning the FDTD, the time-stepping for $\vec{E}$, after elimination of $\vec{H}$, is the standard centered finite difference method, (2.1) with $\theta = 0$ and $\mathbf{S}$ and $\mathbf{M}$ lumped according to trapezoidal integration.

In the *new* version of the hybrid, we assign the implicitness parameter θ on the basis of *elements* rather than edges. This follows the same ideas as the previous successful prescription for the spatial discretization. Thus, the implicitness can be treated as a parameter θ_k for each element $k = 1, ..., K$ where K is the number of elements. We introduce the notation $\mathbf{S}_k$ for the contribution to $\mathbf{S}$ from element k, so that $\mathbf{S} = \sum_{k=1}^{K} \mathbf{S}_k$, and analogously for $\mathbf{M}$. The new algorithm, where θ is assigned to the elements, is

$$\sum_{k=1}^{K} \Bigg(\mathbf{S}_k \left[\theta_k \mathbf{e}^{(n+1)} - (2\theta_k - 1)\mathbf{e}^{(n)} + \theta_k \mathbf{e}^{(n-1)}\right] + \frac{1}{\Delta t^2} \mathbf{M}_k \left[\mathbf{e}^{(n+1)} - 2\mathbf{e}^{(n)} + \mathbf{e}^{(n-1)}\right] \Bigg) = 0, \tag{2.2}$$

where θ_k is chosen $\geq 1/4$ on the implicit elements and zero on the bricks. As will be shown, this not only reduces reflections at the interface, but also makes possible a simple proof of stability.

2.3. **Proof of stability.** Here, we prove stability assuming, for simplicity, that ϵ and μ are constant. The proof relies on bounds for a quadratic form, and first we need the corresponding result for the FDTD part.

2.3.1. *Eigenvalues of the FDTD for one brick element.* To bound the quadratic form, we wish to find bounds for the 12 eigenvalues of the FDTD matrices, for a single element

$$\mathbf{S}_k \mathbf{e} = \lambda \mathbf{M}_k \mathbf{e} \tag{2.3}$$

with $\mathbf{S}_k$ and $\mathbf{M}_k$ lumped. Here, 7 eigenvalues are exactly zero. These correspond to the "potential modes" $\vec{E} = -\nabla\phi$, where the potential ϕ is a trilinear function. The potential can be set to zero at one node, and then there is one eigenmode of (2.3) with $\lambda = 0$ for each of the remaining seven nodes. To determine the remaining five eigenvalues, we studied the eigenvalue problem (2.3) using Mathematica, for a brick with sides h_x, h_y, and h_z in the three coordinate directions. We found the remaining eigenvalues

$$\lambda_8 = \frac{4}{\epsilon\mu}\left(\frac{1}{h_y^2} + \frac{1}{h_z^2}\right), \quad \lambda_9 = \frac{4}{\epsilon\mu}\left(\frac{1}{h_x^2} + \frac{1}{h_z^2}\right), \quad \lambda_{10} = \frac{4}{\epsilon\mu}\left(\frac{1}{h_x^2} + \frac{1}{h_y^2}\right),$$

and the largest eigenvalue is the pair

$$\lambda_{11} = \lambda_{12} = \frac{4}{\epsilon\mu}\left(\frac{1}{h_x^2} + \frac{1}{h_y^2} + \frac{1}{h_z^2}\right) \equiv \lambda_{\max} \tag{2.4}$$

As expected, the largest eigenvalues equal the eigenvalue for the fastest varying exponential function $\exp[j\pi(x/h_x + y/h_y + z/h_z)]$ on a uniform, infinite grid. This mode gives the Courant-Friedrichs-Levy (CFL) limit for the FDTD time step

$$\Delta t \leq \Delta t_{\mathrm{CFL}} = 2/\sqrt{\lambda_{\max}} \tag{2.5}$$

If $h_x = h_y = h_z = h$, (2.5) gives the usual CFL limit, $h/c\sqrt{3}$. The explicit expression (2.4) for the largest eigenvalues gives the following inequality, valid for any complex vector $\mathbf{e}$

$$\mathbf{e}^H \mathbf{S}_k \mathbf{e} \leq \lambda_{\max} \mathbf{e}^H \mathbf{M}_k \mathbf{e} \tag{2.6}$$

where $\mathbf{e}^H$ is the complex transpose of $\mathbf{e}$.

2.3.2. *Quadratic form for the hybrid algorithm.* We are now in a position to prove stability by the von Neumann method. Let $\tilde{\mathbf{e}}$ be a complex eigenmode of the new hybrid algorithm (2.2), and assume that it has a growth factor ρ such that $\mathbf{e}^{(n)} = \rho^n\tilde{\mathbf{e}}$. For this mode Eq. (2.2) gives:

$$\sum_{k=1}^{K}\left(\mathbf{S}_k\left[\theta_k\rho^2-(2\theta_k-1)\rho+\theta_k\right]+\frac{1}{\Delta t^2}\mathbf{M}_k\left[\rho^2-2\rho+1\right]\right)\tilde{\mathbf{e}}=0. \tag{2.7}$$

Stability is equivalent to $|\rho|\leq 1$ for all modes $\tilde{\mathbf{e}}$. With the substitution $\rho=(1+\zeta)/(1-\zeta)$ this condition becomes $\Re(\zeta)\leq 0$, and (2.7) is transformed into:

$$\sum_{k=1}^{K}\tilde{\mathbf{e}}^H\mathbf{S}_k\tilde{\mathbf{e}}=-\zeta^2\sum_{k=1}^{K}\tilde{\mathbf{e}}^H\left[\frac{4}{\Delta t^2}\mathbf{M}_k+\mathbf{S}_k\left(4\theta_k-1\right)\right]\tilde{\mathbf{e}}. \tag{2.8}$$

Since all the matrices are Hermitian, ζ^2 is real. Furthermore, since the left-hand side is non-negative stability follows if the sum on the right-hand side is positive for all $\tilde{\mathbf{e}}$. This sum can be split into the contribution from the explicit and implicit elements. The contribution from the implicit elements is non-negative if $\theta_k\geq 1/4$ everywhere on this grid. By virtue of (2.6), the contribution from the explicit elements is non-negative if the time step satisfies the CFL condition (2.5) for the FDTD. Therefore, the new implicit-explicit algorithm (2.2), with $\theta\geq 1/4$ on the implicit elements, is stable for time steps up to the stability limit of the FDTD.

Stability of a similar implicit-explicit hybrid in acoustics was proven by Belytschko and Mullen [15]. These authors used the trapezoidal integration rule in time on the implicit grid, with the displacement $\vec{\xi}$ and velocity $\vec{v}=\partial\vec{\xi}/\partial t$ placed on the same time levels. This is equivalent to the implicit scheme (2.1) with $\theta = 1/4$. An extensive overview over different time-stepping schemes used in computational mechanics, including explicit-implicit hybrids, is given by Hughes [16].

3. Numerical results

One possible drawback of a hybrid method is reflections at the interfaces between the two types of grid. Here, we study such reflections for the new hybrid method and compare with our original scheme [8]. We also compare the hybrid to the FDTD with the staircase approximation, for scattering from a perfect electrically conducting (PEC) sphere.

3.1. **Reflection at grid interfaces.**

A simple arrangement to test the reflection at the FEM-FDTD interface is to inject a TE_{10} mode into a waveguide. This is illustrated in Fig. 2, where a thin layer of tetrahedrons and pyramids is embedded in an FDTD grid of cubes. Figure 1 shows the cross section of the waveguide around the implicit layer for such a test. The width of the waveguide is twice its height.

The injected wave has the time dependence $E_y(t)=\exp[-(t-t_0)^2/d_0^2]\sin(2\pi ft)$, where $t_0 = 6.25/f_c$, $d_0 = 2.5/f_c$, $f=\sqrt{2}f_c$ and f_c is the cutoff frequency for the TE_{10} mode. The power reflection coefficients are shown as contour plots in Fig. 3 and Fig. 4 for the original

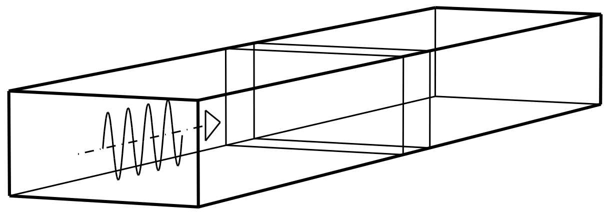

FIGURE 2. Waveguide with the incident pulse traveling towards the implicit layer.

and new hybrid scheme when the waveguide is discretized by 10×5 FDTD cells in the cross section.

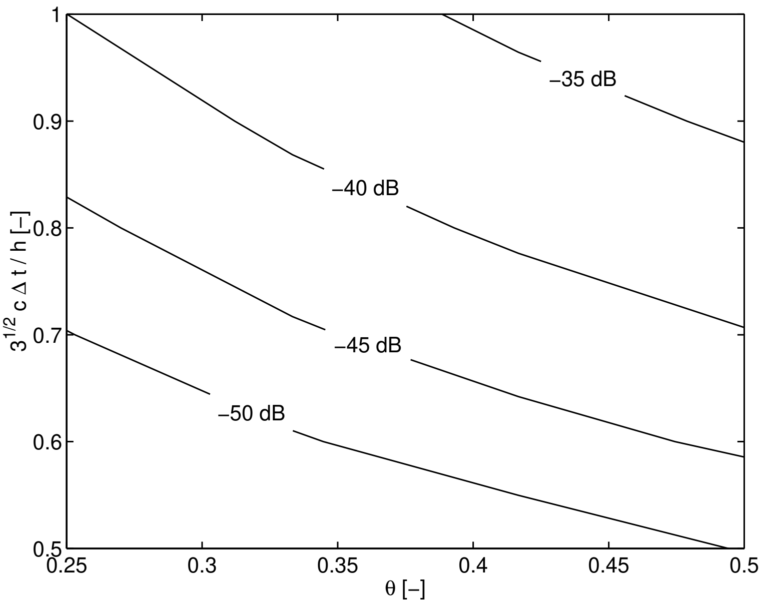

FIGURE 3. Level contours of the power reflection coefficient in the waveguide test for the original scheme with 14 cells per wavelength.

The reflection for the new hybrid is much less sensitive to the choice of θ and Δt than the original scheme. For the maximum FDTD time step and $\theta = 1/4$, the new hybrid gives a power reflection coefficient below -46 dB, while the original hybrid gives -40 dB.

Riley [17] proposed another modification of the hybrid method, namely to apply trapezoidal integration over the bases of the pyramids. Figure 5 shows how the power reflection coefficient depends on resolution for $\theta = 1/4$ and $\Delta t = \Delta t_{\mathrm{CFL}}$ and all four combinations of discretization techniques at the interface between the explicit and implicit grids. Here, the dimensions of the waveguide were kept fixed, while the thickness of the layer of tetrahedrons and pyramids was constant in number of cells. Results for the original and new

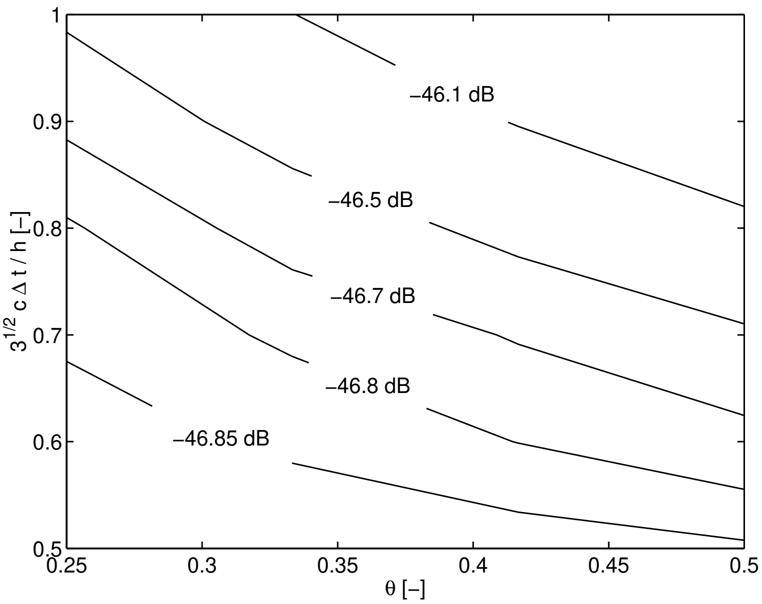

FIGURE 4. Level contours of the power reflection coefficient in the waveguide test for the new hybrid scheme with 14 cells per wavelength.

hybrid scheme are indicated by circles and squares, respectively, while dashed and solid lines correspond to exact and trapezoidal integration over the base of the pyramids, respectively. A least square fit to our results for $\lambda/h \geq 17$ shows that the power reflection coefficient varies as $h^{5.7}$

3.2. **Scattering from PEC sphere.** We have also made tests comparing the hybrid to the FDTD for scattering by a PEC sphere. The hybrid was run with $\theta_k = 1/4$ on the tetrahedrons and pyramids and the time step at the CFL limit for the FDTD. The PETSc [18] sparse matrix package was used to solve the implicit equations in the FEM region. The inversion is done efficiently by the conjugate gradient method with a zero-fill-in ILU-preconditioner. The residual is reduced by about 10^{-6} with nine iterations.

An incident plane wave $E_{\rm inc}(t) = E_0 \exp[-(t-t_0)^2/d_0^2] \sin[\omega_0(t-t_0)]$ is imposed at a Huygens surface [2]. The wavenumber vector of the incident plane wave is parallel to one of the Cartesian axes of the FDTD grid. The radiation pattern is obtained by means of a near-to-far-field (NTF) transformation [2]. We apply an NTF transformation using third order Lagrange interpolation and four point Gauss quadrature. It converges with an $O(h^4)$ error and gives a maximum error of 0.05 % when $\lambda/h = 18$. The scattered wave is absorbed at the outer boundary by a "sponge layer" [19].

In [20], our original hybrid was validated with this setup against the analytic results for a PEC sphere. Here we apply the same test to the new version. The bistatic RCS for a sphere of radius $a = 1$ m is computed on three different meshes with FDTD cell size $h = n/15\sqrt{3}$ m for $n = 9$, 6 and 4. The hybrid grids are constructed as described in [8]

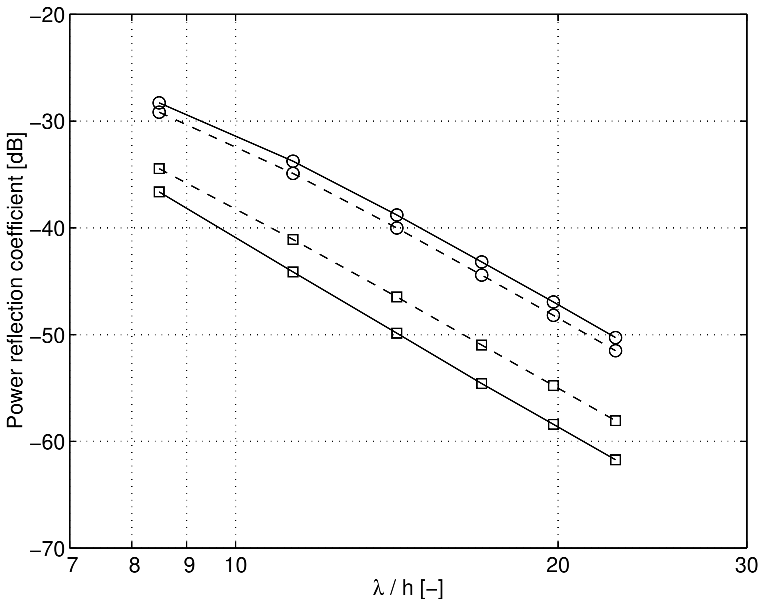

FIGURE 5. Power reflection coefficient for $\theta = 1/4$ and $\Delta t = \Delta t_{\mathrm{CFL}}$ versus number of cells per wavelength. The new scheme is shown as squares, the original as circles. Dashed lines indicate exact integration over the pyramids, while solid lines indicate trapezoidal integration.

and parts of the grid for $n = 9$ are shown in Fig. 6. In this particular case, we generated tetrahedrons with edges of the length roughly equal to the corresponding FDTD cell size h. (For all resolutions, the average length of a tetrahedron edge is within 4% from h and the standard deviation is 20-23% of h). Furthermore, we kept the thickness of the FEM grid constant in terms of cells when the resolution was increased and the average thickness was slightly below $2h$. Consequently, the fraction of the computational effort spent on the FEM region is proportional to h for high resolutions. Although it is not needed for this particular test case, we emphasize that our hybrid allows local refinement of the FEM grid without reduction of the global time-step. Such refinement can be necessary to resolve small geometrical details or the field in the vicinity of a singularity.

The wavelength is $\lambda = 4.16$ m ($ka = 1.5$) and the time constants are $t_0 = 1.73 \cdot 10^{-8}$ s, $d_0 = 6.00 \cdot 10^{-9}$ s. The relative error $e(h) = ||\sigma_n - \sigma_a||_2/||\sigma_a||_2$ is shown in Fig. 7 by circles and squares for the original and the new hybrid scheme, respectively, using exact integration for the pyramids. Here σ_n and σ_a are the numerically computed and analytic bistatic RCS, respectively, and $||\cdot||_2 = [\int_\Omega (\cdot)^2 d\Omega]^{1/2}$. The improved hybrid scheme reduces the error by 20-30% compared to the original version. With trapezoidal integration over the bases of the pyramids the relative error increased 2-3% for the original and 3-5% for the new hybrid scheme.

Least square fits to the model $e(h) = ch^\alpha$ are shown by the dashed lines in Fig. 7, and for the original and the new hybrid scheme we found $\alpha \simeq 2.02$ and $\alpha \simeq 1.84$, respectively.

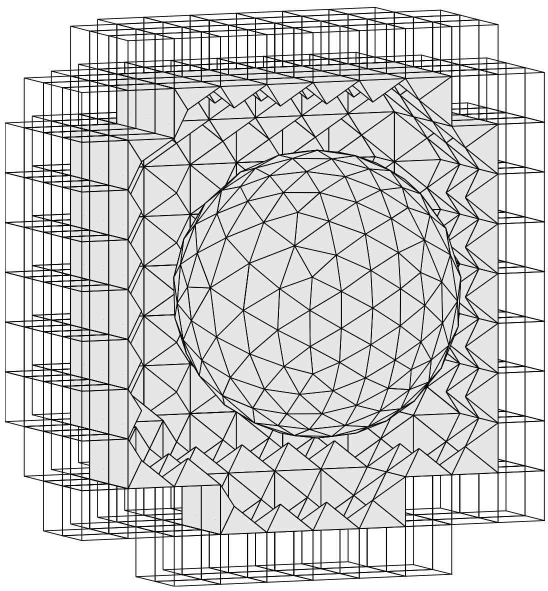

FIGURE 6. Parts of the hybrid grid for the PEC sphere when $n = 9$. The discretized surface of the sphere is shown together with some of the pyramids. The first layer of FDTD cubes, connecting to the bases of the pyramids, is indicated by lines.

One effect that contributes to deviations from second order convergence is the non-uniform refinement of the unstructured grid.

Table 1 shows the number of cells required, for 5% accuracy in the bistatic RCS measured by the L_2 (rms) and L_∞ (max) norms with the original and the improved hybrid scheme.

TABLE 1. Required resolution λ/h for 5% accuracy in the bistatic RCS for the PEC sphere.

	Original hybrid	Improved hybrid
5% accuracy in L_2-norm	16.2	13.5
5% accuracy in L_∞-norm	20.7	18.9

We have applied this test to the stair-cased FDTD. Some rather arbitrary decisions have to be taken for the stair-casing. Figure 7 shows results obtained with three different criterions for an FDTD cell to be PEC: (a) at least one corner of the cell is inside the physical sphere ($\triangle$), (b) the midpoint of the cell is inside the physical sphere ($\diamondsuit$) and (c) all corners of the cell are inside the physical sphere ($\bigtriangledown$).

The errors for the stair-cased FDTD are about 5 - 60 times larger than those for the hybrid scheme. At all resolutions, the best FDTD result is obtained with method (c) where the FDTD cubes are modeled as conducting only when they are *completely* inside

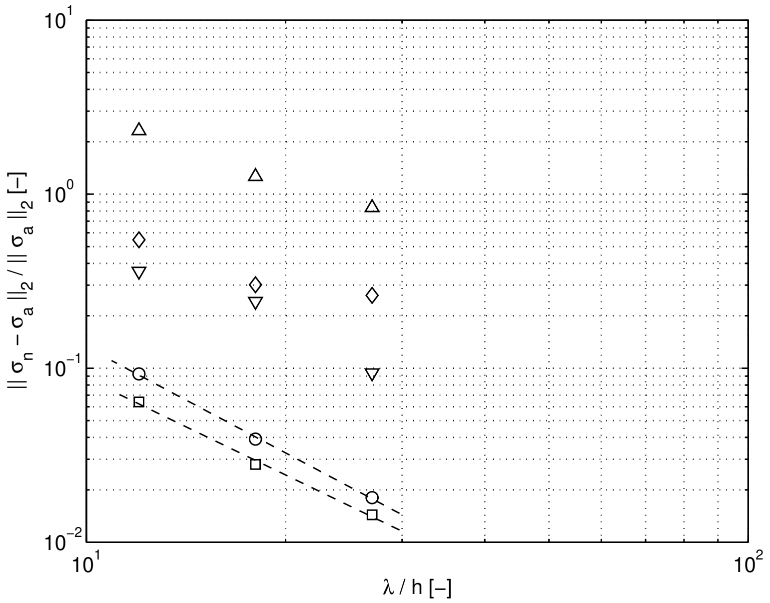

FIGURE 7. The relative error in the bistatic RCS for a PEC sphere is shown by circles and squares for the original and the new hybrid scheme, respectively, and fits to the model $e(h) = ch^{\alpha}$ are shown by the dashed lines. For the stair-cased FDTD we used three different criterions for an FDTD cell to be PEC: (a) at least one corner of the cell is inside the physical sphere ($\triangle$), (b) the midpoint of the cell is inside the physical sphere ($\diamondsuit$) and (c) all corners of the cell are inside the physical sphere ($\bigtriangledown$).

the sphere. This gives errors that are 5 - 9 times larger than for the hybrid. To achieve a given relative error, the best FDTD (c) needs more than twice the linear resolution of the hybrid. Consequently, for the same accuracy as the FEM-FDTD hybrid method, the best FDTD (c) needs roughly 20 times more execution time and 10 times more memory. Moreover, the stair-cased FDTD schemes do not show a very clear order of convergence, which reduces the predictive power of extrapolation.

Table 2 shows the number of mega floating point operations (Mflops) per time-step for the FDTD- and FEM-part of the computation. Here, one flop is defined as one real number operation of the type: multiplication, division, addition or subtraction. The computational cost is almost six times higher for the sponge layer compared to the standard FDTD in homogeneous space, which is included in Tab. 2. For the FEM-part, the initial costs associated with the setup of the linear system of equations (computation of the element matrices excluded) and the computation of the preconditioner are amortized equally over all time-steps. It should be mentioned that the total number of time-steps is rather small for this particular problem, e.g. 206 time-steps for $n = 9$, and that, for all resolutions, the iterative solver used about 15 iterations for each time-step. It is possible to reduce the flops per time-step for the FEM-part, keeping sufficient accuracy. Note that the number of operations for the FEM-region, relative to the FDTD-region, decreases as the resolution increases and 10% of the flops are spent on the FEM-part for the highest resolution with 27 points per wavelength.

TABLE 2. The number of mega floating point operations (Mflops) per time-step for the FDTD- and FEM-part of the computation.

n	FDTD	FEM
9	16	6.0
6	56	11
4	189	21

3.3. **Scattering from the FEM-FDTD interface.** To investigate the scattering at the FEM-FDTD interface, we replaced the interior of the sphere by vacuum, discretized by tetrahedrons. The computed RCS of the empty grid is shown in Fig. 8 with respect to λ for different discretizations at the explicit-implicit interface. Here, the FDTD cell size is fixed to $h = \sqrt{3}/5$. (Since, in this figure, the quantity that varies is the wavelength, rather than the grid size, and the geometry is fixed, the result cannot not be interpreted strictly as a convergence test.) The solid curves with circles and squares correspond to the original and the new scheme, respectively. Our new scheme for time-stepping significantly reduces the scattering from the grid interface. According to Fig. 8, the improved hybrid reduces the RCS of the empty grid about 10 dB for $\lambda/h > 25$. For 12 cells per wavelength, the computed RCS of the empty grid was at least 35 dB below that of the conducting sphere in all directions. Trapezoidal integration over the bases of the pyramids changes the RCS of the empty grid less than 1 dB.

4. Conclusion

We have presented an improved version of the stable FEM-FDTD hybrid [8] and given a proof of stability for the new explicit-implicit time integration. The new hybrid reduces the reflection from the interface between the FEM and FDTD grids.

The standard FDTD scheme, with the staircase approximation, was compared with the hybrid for scattering from a PEC sphere. The hybrid converges towards the exact solution with an $O(h^2)$ error. For scattering from a conducting sphere with $ka = 1.5$ the hybrid achieves a root mean square accuracy of 5% with 13.5 cells per wavelength. For the FDTD, three different approaches for the stair-casing gave significantly different results. The best FDTD results were obtained when only the cubes completely inside the conductor were modeled as conducting. This gave errors that were about 5 - 9 times higher than for the hybrid scheme. With other choices for when to make an FDTD cell a conductor, the error could be as much as 60 times that of the hybrid. None of the tested stair-casing strategies for the FDTD produced a very clear order of convergence. To obtain results of comparable accuracy as the hybrid, the FDTD needs at least twice as many cells per wave-length as the hybrid. Since the number of the operations for the FEM part of the hybrid is typically

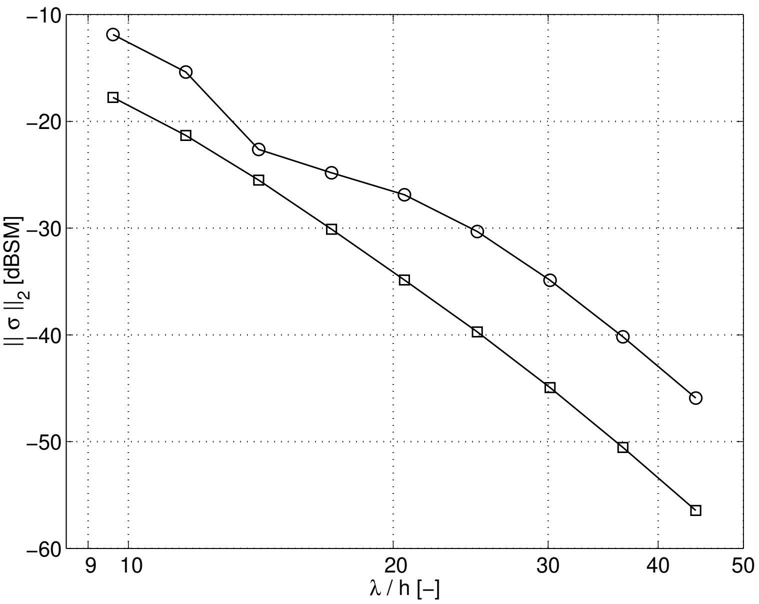

FIGURE 8. The norm of the bistatic RCS for an empty sphere versus number of points per wavelength. Results for the new hybrid are shown as squares and for the original hybrid as circles.

less than for the FDTD part, the hybrid algorithm significantly reduces the total number of operations needed for a given accuracy.

We conclude that the hybrid method works robustly and combines the main advantages of the FDTD with those of edge finite elements on unstructured grids. In comparison to the stair-cased FDTD, the hybrid method is significantly more efficient when the geometry contains curved surfaces.

5. Acknowledgment

This work was supported in part by grants from National Graduate School of Scientific Computing (NGSSC) and the Technical Research Foundation (TFR). The Center of Computational Electromagnetics is supported by the School of Electrical and Computer Engineering at Chalmers University. The research has profited in many ways from a collaboration with the Finite Element Center at Chalmers University.

References

[1] K. S. Yee, "Numerical solution of initial boundary value problems in isotropic media," *IEEE Trans. Antennas Propagat.* **14**, 302 (1966).

[2] A. Taflove, *Computational Electrodynamics: The Finite-Difference Time-Domain Method* (Artech House, Norwood, MA, 1995).

[3] J. Jin, *The Finite Element Method in Electromagnetics* (Wiley, New York, 1993).

[4] J. C. Nédélec, "Mixed finite elements in R^3," *Numer. Math.* **35**, 315 (1980).

[5] K. S. Yee, J. S. Chen and A. H. Chang, "Numerical Experiments On PEC Boundary Condition and Late Time Growth Involving the FDTD/FDTD and FDTD/FVTD Hybrid," *IEEE Antennas Propagat. Soc. Int. Symp.* **1**, 624 (1995).
[6] R. B. Wu and T. Itoh, "Hybrid Finite-Difference Time-Domain Modeling of Curved Surfaces Using Tetrahedral Edge Elements," *IEEE Trans. Antennas Propagat.* **45**, 1302 (1997).
[7] A. Monorchio and R. Mittra, "A hybrid Finite-Element Finite-Difference Time-Domain (FE/FDTD) technique for solving complex electromagnetic problems," *IEEE Microw. Guided Wave Lett.* **8**, 93 (1998).
[8] T. Rylander and A. Bondeson, "Stable FEM-FDTD hybrid method for Maxwell's equations," *Comput. Phys. Comm.* **125**, 75 (2000).
[9] K. H. Dridi, J. S. Hesthaven and A. Ditkowski, "Staircase-Free Finite-Difference Time-Domain Formulation for General Materials in Complex Geometries," *IEEE Trans. Antennas Propagat.* **49** 749 (2001).
[10] T. A. Driscoll and B. Fornberg, "Block pseudospectral methods for Maxwell's equations II: two-dimensional, discontinuous-coefficient case," *SIAM J. Sci. Comput.* **21**, 1146 (1999).
[11] P. Thoma and T. Weiland, "Numerical Stability of Finite Difference Time Domain Methods," *IEEE Trans. Magnetics* **34**, 2740 (1998).
[12] R. Schuhmann and T. Weiland, "Stability of the FDTD Algorithm on Nonorthogonal Grids Related to the Spatial Interpolation Scheme," *IEEE Trans. Magnetics* **34**, 2751 (1998).
[13] M. Celuch-Marcysiak and W. K. Gwarek, "Generalized TLM Algorithms with Controlled Stability Margin and Their Equivalence with Finite-Difference Formulations for Modified Grids," *IEEE Trans. Microwave Theory Tech.* **43**, 2081 (1995).
[14] J. F. Lee, R. Lee and A. Cangellaris, "Time-Domain Finite-Element Methods," *IEEE Trans. Antennas Propagat.* **45**, 430 (1997).
[15] T. Belytschko and R. Mullen, "Stability of Explicit-Implicit Mesh Partitions in Time Integration," *International Journal for Numerical Methods in Engineering* **12**, 1575 (1978).
[16] T. J. R. Hughes, *The finite element method: linear static and dynamic finite element analysis* (Prentice-Hall, Englewood Cliffs, NJ, 1987).
[17] D. J. Riley, "Transient Finite-Elements for Computational Electromagnetics: Hybridization with Finite Differences, Modeling Thin Wires and Thin Slots, and Parallel Processing," *Applied Computational Electromagnetics Society (ACES) Symposium* (2001).
[18] S. Balay, W. D. Gropp, L. C. McInnes, and B. F. Smith, "PETSc home page," `http://www.mcs.anl.gov/petsc` (1998).
[19] P. G. Petropoulos, L. Zhao, and A. C. Cangellaris, "A Reflectionless Sponge Layer Absorbing Boundary Condition for the Solution of Maxwell's Equations with High-Order Staggered Finite Difference Schemes," *J. Comput. Phys.* **139**, 184 (1998), doi:10.1006/jcph.1997.5855.
[20] T. Rylander and A. Bondeson, "Application of Stable FEM-FDTD Hybrid to Scattering Problems," *IEEE Trans. Antennas Propagat.* (2002).

Chalmers Finite Element Center Preprints

2000–01 *Adaptive finite element methods for the unsteady Maxwell's equations*
Johan Hoffman

2000–02 *A multi-adaptive ODE-solver*
Anders Logg

2000–03 *Multi-adaptive error control for ODEs*
Anders Logg

2000–04 *Dynamic computational subgrid modeling* (Licentiate Thesis)
Johan Hoffman

2000–05 *Least-squares finite element methods for electromagnetic applications* (Licentiate Thesis)
Rickard Bergström

2000–06 *Discontinuous galerkin methods for incompressible and nearly incompressible elasticity by Nitsche's method*
Peter Hansbo and Mats G. Larson

2000–07 *A discountinuous Galerkin method for the plate equation*
Peter Hansbo and Mats G. Larson

2000–08 *Conservation properties for the continuous and discontinuous Galerkin methods*
Mats G. Larson and A. Jonas Niklasson

2000–09 *Discontinuous Galerkin and the Crouzeix-Raviart element: application to elasticity*
Peter Hansbo and Mats G. Larson

2000–10 *Pointwise a posteriori error analysis for an adaptive penalty finite element method for the obstacle problem*
Donald A. French, Stig Larson and Ricardo H. Nochetto

2000–11 *Global and localised a posteriori error analysis in the maximum norm for finite element approximations of a convection-diffusion Problem*
Mats Boman

2000–12 *A posteriori error analysis in the maximum norm for a penalty finite element method for the time-dependent obstacle problem*
Mats Boman

2000–13 *A posteriori error analysis in the maximum norm for finite element approximations of a time-dependent convection-diffusion problem*
Mats Boman

2001–01 *A simple nonconforming bilinear element for the elasticity problem*
Peter Hansbo and Mats G. Larson

2001–02 *The $\mathcal{LL}^*$ finite element method and multigrid for the magnetostatic problem*
Rickard Bergström, Mats G. Larson, and Klas Samuelsson

2001–03 *The Fokker-Planck operator as an asymptotic limit in anisotropic media*
Mohammad Asadzadeh

2001–04 *A posteriori error estimation of functionals in elliptic problems: experiments*
Mats G. Larson and A. Jonas Niklasson

2001–05 *A note on energy conservation for Hamiltonian systems using continuous time finite elements*
Peter Hansbo

2001–06 *Stationary level set method for modelling sharp interfaces in groundwater flow*
Nahidh Sharif and Nils-Erik Wiberg

2001–07 *Integration methods for the calculation of the magnetostatic field due to coils*
Marzia Fontana

2001–08 *Adaptive finite element computation of 3D magnetostatic problems in potential formulation*
Marzia Fontana

2001–09 *Multi-adaptive galerkin methods for ODEs I: theory & algorithms*
Anders Logg

2001–10 *Multi-adaptive galerkin methods for ODEs II: applications*
Anders Logg

2001–11 *Energy norm a posteriori error estimation for discontinuous Galerkin methods*
Roland Becker, Peter Hansbo, and Mats G. Larson

2001–12 *Analysis of a family of discontinuous Galerkin methods for elliptic problems: the one dimensional case*
Mats G. Larson and A. Jonas Niklasson

2001–13 *Analysis of a nonsymmetric discontinuous Galerkin method for elliptic problems: stability and energy error estimates*
Mats G. Larson and A. Jonas Niklasson

2001–14 *A hybrid method for the wave equation*
Larisa Beilina, Klas Samuelsson and Krister Åhlander

2001–15 *A finite element method for domain decomposition with non-matching grids*
Roland Becker, Peter Hansbo and Rolf Stenberg

2001–16 *Application of stable FEM-FDTD hybrid to scattering problems*
Thomas Rylander and Anders Bondeson

2001–17 *Eddy current computations using adaptive grids and edge elements*
Y. Q. Liu, A. Bondeson, R. Bergström, C. Johnson, M. G. Larson, and K. Samuelsson

2001–18 *Adaptive finite element methods for incompressible fluid flow*
Johan Hoffman and Claes Johnson

2001–19 *Dynamic subgrid modeling for time dependent convection–diffusion–reaction equations with fractal solutions*
Johan Hoffman

2001–20 *Topics in adaptive computational methods for differential equations*
Claes Johnson, Johan Hoffman and Anders Logg

2001–21 *An unfitted finite element method for elliptic interface problems*
Anita Hansbo and Peter Hansbo

2001–22 *A P^2–continuous, P^1–discontinuous finite element method for the Mindlin-Reissner plate model*
Peter Hansbo and Mats G. Larson

2002–01 *Approximation of time derivatives for parabolic equations in Banach space: constant time steps*
Yubin Yan

2002–02 *Approximation of time derivatives for parabolic equations in Banach space: variable time steps*
Yubin Yan

2002–03 *Stability of explicit-implicit hybrid time-stepping schemes for Maxwell's equations*
Thomas Rylander and Anders Bondeson

These preprints can be obtained from

`www.phi.chalmers.se/preprints`